Asian Journal of Pharmaceutical Sciences 13 (2018) 326–335

Available online at www.sciencedirect.com

ScienceDirect

journal homepage: www.elsevier.com/locate/AJPS

Original Research Paper

Enhanced digestion inhibition and mucus penetration of F127-modified self-nanoemulsions for improved oral delivery☆

Wenyi Song[a,b], *Yuting Yang*[a,b], *Miaorong Yu*[b,c], *Quanlei Zhu*[b,c], *Mohammadali Soleimani Damaneh*[c,d], *Haijun Zhong*[a,*], *Yong Gan*[b,c,**]

[a] *Department of Pharmacy, Medical College of Nanchang University, 461 Bayi Road, Nanchang 330066, China*
[b] *Shanghai Institute of Materia Medica, Chinese Academy of Sciences, No. 501 Haike Road, Shanghai 201203, China*
[c] *University of Chinese Academy of Sciences, NO.19A Yuquan Road, Beijing 100049, China*
[d] *Division of Anti-tumor Pharmacology, State Key Laboratory of Drug Research, Shanghai Institute of Materia Medica, Chinese Academy of Sciences, 555 Zuchongzhi Road, Shanghai 201203, China*

ARTICLE INFO

Article history:
Received 23 January 2018
Revised 1 March 2018
Accepted 5 March 2018
Available online 17 March 2018

Keywords:
Self-nanoemulsifying system (SNEs)
Oral absorption
Enzymatic degradation
Mucus penetration
Pluronic® F127

ABSTRACT

Self-nanoemulsifying systems (SNEs) have excellent ability to improve the solubility of poorly water-soluble drugs (PWSD). However, SNEs are likely to be degraded in gastrointestinal (GIT) when their surface is recognized by lipase/co-lipase enzyme complex, resulting in rapid release and precipitation of encapsulated drugs. The precipitates are then captured and removed by intestinal mucus, reducing the delivery efficacy of SNEs. Herein, the amphiphilic polymer Pluronic® F127 was incorporated into long and short-chain triglycerides (LCT, SCT) based SNEs to diminish the recognition and therefore minimized their degradation by enzymes and clearance by mucus. The SNEs were characterized in terms of particle size, zeta potential and stability. Ex vivo multiple particles tracking studies were performed by adding particle solution into fresh rat mucus. Cellular uptake of SNEs were conducted by using E12 cells, the absorption and distribution in small intestine were also studied after oral administration in male Sprague-Dawley (SD) rats. The *in vitro* digestion rate of SNEs were found to be in following order SCT-SNE > SCT-F127-SNE > LCT-SNE > LCT-F127-SNE. Moreover, the LCT-F127-SNE was found to be most effective in enhancing cellular uptake, resulting in 3.5-fold, 2.1-fold and 1.7-fold higher than that of SCT-SNE, LCT-SNE and SCT-F127-SNE, respectively. After incubating the SNE with E12 cells, the LCT-F127-SNE exhibited the highest amount regarding both mucus penetration and cellular uptake, with an uptake amount number (via bicinchoninic acid (BCA) analysis) of 3.5-fold, 2.1-fold and 1.7-fold higher than that of SCT-SNE, LCT-SNE and SCT-F127-SNE, respectively. The *in vivo* results

☆ Peer review under responsibility of Shenyang Pharmaceutical University.

* Corresponding author at: Department of Pharmacy, Medical College of Nanchang University, 461 Bayi Road, Nanchang 330066, China. Tel.: 86-21-20231000-1425

** Corresponding author at: Shanghai Institute of Materia Medica, Chinese Academy of Sciences, No. 501 Haike Road, Shanghai 201203, China. Tel.: 86-0791-86361839

E-mail addresses: zhonghj@ncu.edu.cn (H. Zhong), ygan@simm.ac.cn (Y. Gan).

https://doi.org/10.1016/j.ajps.2018.03.001

revealed that orally administered LCT-F127-SNE could significantly increase the bioavailability of Cyclosporine A (CsA), which was approximately 2.43-fold, 1.33-fold and 1.80-fold higher than that of SCT-SNE, SCT-F127-SNE and LCT-SNE, respectively. We address in this work that F127-modified SNEs have potentials to improve oral drug absorption by significantly reducing gastrointestinal enzymatic degradation and simultaneously enhancing mucus penetration.

1. Introduction

Oral drug delivery is the most acceptable administration route for patients. However, a large number of pharmaceuticals, such as poorly water-soluble drugs (PWSD), cannot exhibit therapeutic effects after oral administration [1–3]. Self-nanoemulsifying systems (SNEs), possessing high loading capacity of PWSD, have been proven effective to increase the bioavailability of hydrophobic drugs [4,5]. They have the ability to protect PWSD in the harsh gastrointestinal (GIT) environment as well as minimize the influence of food [4,6]. For example, Porter et al., found that lipid-based formulations (LBFs) could effectively improve hydrophobic drug absorption by changing the type of lipid or surfactant ratio to minimize lipolysis [7–9]. Junjiang Fu et al., designed a novel nanoemulsion formulation, consisting of soy-lecithin, tween-80, polyethylene glycol 400, isopropyl myristate, and water (1:2:1.5:3.75:8.25, w/w), to improve the oral bioavailability of baicalin [10]. However, SNEs can be digested by the lipase superfamily of active enzymes, which would lead to nonspecific adsorption of the enzyme complex on the surface of an emulsified oil droplet, resulting in the dramatic decrease of drug absorption [11–13]. Meanwhile, their low mucus penetration ability probably increases the possibility of mucus entrapment, which leads to their further degradation by lipases in the mucus layer and rapid clearance by mucociliary system. Therefore, the traditional approaches of SNEs to enhancing the bioavailability of PWSD need further improvement, enabling them to be resistant to luminal digestion and capable of traversing the mucus layer rapidly.

In the past decade, it has been proved that mucus is a substantial barrier to nanoparticles (NPs) [14]. The intestinal mucus with tenacious mesh structure is mainly composed of mucin protein, which can impede foreign particles from reaching the underlying epithelia [15,16]. The limited permeability of particles through mucus can further lead to their clearance from the GIT, resulting in poor absorption [17]. It has been reported that NPs modified with polymers, which has long hydrophilic chain, such as Pluronic® F127 or polyethylene glycol (PEG) polymers, could exhibit excellent mucus diffusion ability [14,18]. Therefore, we hypothesize that SNEs will efficiently overcome both lipases and mucus barriers, if they are decorated with hydrophilic polymers.

The purpose of present study is to explore an innovative SNE to improve the oral bioavailability of PWSD. Herein, we used short-chain triglycerides (SCT) and long-chain triglycerides (LCT) to prepare bare SNEs, and these were further coated with F127 to enhance their stability and hydrophilicity. The effect of F127 coating on lipid digestion and mucus permeation of SNEs were examined *in vitro*, and their cellular uptake and absorption in the small intestinal loops were further investigated by confocal imaging. The improved oral absorption of Cyclosporine A (CsA) by F127-SNEs were confirmed in Sprague–Dawley rats. We herein illustrate that the strategy to enhance digestion inhibition and mucus penetration will open new vista for the applications of SNEs for oral delivery in the future.

2. Materials and methods

2.1. Materials

CsA and cyclosporine D (CsD) were purchased from the Fujian Kerui Pharmaceutical Co., Ltd. (Fujian, China). Maisine CC (LCT) was purchased from Tieling Beiya Medical Oil Co., Ltd. (Tieling, Liaoning, China). Glyceryl tributyrate (SCT) was purchased from Beijing Xizhong Chemical Plant (Beijing, China). Cremophor EL was purchased from BASF AG (Ludwigshafen, Germany), porcine pancreatic lipase (1:250), Taurocholic sodium (NaTC), Opti-mum cutting Temperature Compound (OTC) and 4% Paraformaldehyde were purchased from Melone Pharmaceutical Co., Ltd. (Dalian, China). 2-(4-amidinophenyl)−6-indolecarbamidine-dihydrochloride (DAPI) and 1,1′-dioctadecyl-3,3,3′,3′-tetramethylindocarbocyanine perchlorate (DiI) were purchased from Beyotime BioTechnology (Shanghai China). Alexa Fluor 488-conjugated WGA was obtained from Sigma Aldrich (USA). HT29-MTX-E12 (E12) cells cultured for 14–18 days were supplied by the ADME Department of Novo Nordisk A/S, Denmark. Acetonitrile, methanol, n-hexane, and tert–butyl methyl ether of high-performance liquid chromatography (HPLC) grade were obtained from the Tedia Company Inc. (Fairfield, Ohio, USA). Tris-(hydroxymethyl) aminomethane, maleic acid, ethanol, glycerol, propylene glycol, calcium chloride and sodium chloride were all purchased from the Sinopharm Chemical Reagent Co., Ltd. (Shanghai, China). All other reagents were of analytical grade.

2.2. Formulation preparation

The compositions of all SNE formulations were shown in Supplementary Table S1. Each SNE is consisted of ethanol, 1,2-propanediol, surfactant and oil phase (1:1:4:4, w/w). Briefly,

F127 (25 mg) was firstly dissolved in the mixture of co-solvents (50 mg ethanol and 50 mg 1,2-propanediol). (CsA or DiI was dissolved simultaneously at the first step for pharmacokinetic study and fluorescent detection experiments, respectively.) Then, cremophor EL (200 mg) was introduced and the mixture was added to the oil phase (200 mg, either SCT or LCT), followed by vibrating for 60 s at room temperature to make it homogeneity. Finally, formulations were dispersed in phosphate buffer saline (PBS) before use.

2.3. Characterization of formulation

The SNE formulations were diluted to 100 times with PBS for particle size, PDI and zeta-potential determination. The particle size, PDI and zeta potential of SNEs formulations were investigated by using dynamic light scattering (DLS, Nano ZS, Malvern, UK).

2.4. Stability of fluorescently labeled SNEs

The *in vitro* stability was measured by monitoring the particle size, PDI, and fluorescence intensity of DiI in PBS (pH 7.4) and biorelevant media at 37 °C for 24 h using a shaking water bath (The concentration of dye was 0.3 mg/ml). The biorelevant media included simulated gastric fluid (SGF) and simulated intestinal fluid (SIF). All the media were prepared according to previously reported [19,20]. SGF was composed of 0.2% sodium chloride (NaCl) (w/v) and 0.32% pepsin (w/v), and the pH was adjusted to 1.2 by slowly adding 0.1 M HCl. SIF was composed of 0.68% monobasic potassium phosphate (KH_2PO_4) (w/v) and 1% pancreatin (w/v), and the pH was adjusted to 6.8 by 0.1 M NaOH.

2.5. Digestion study

2.5.1. Lipid digestion rate

Digestion study were conducted by using an *in vitro* lipid digestion model with slight modifications [12,21]. Each 100 mg SNE formulation was added to the round-bottomed flask containing 19 mL 50 mM Tri-maleate digestion buffer (pH 7.5). Digestion study were allowed to start by adding 1 mL 10% (w/v) porcine pancreatic lipase solution (4000 tributyrin units/mL). Then NaOH solution (1 M) was added when pH dropped at 7.45 during digestion to maintain the pH at 7.50 ± 0.05. The volume of added NaOH solution and time point were recorded. The digestion system was agitated by using a magnetic stirring apparatus at 37 °C. The reaction was terminated when the pH could not drop below 7.45 units during 30 min.

2.5.2. Sample preparation and HPLC analysis of in vitro digested samples

Five mL aliquots of the post-digestion mixture were centrifuged (25,000 g, 30 min, 37 °C) to separate pellet phase and aqueous phase. Each phase was dissolved in 10 mL of tetrahydrofuran-water (4:1 (v/v)). And 10 μL of the solution was injected into the HPLC system. The HPLC condition is described in 2.10. Pharmacokinetic study.

2.6. Multiple particle tracking

We euthanized male Sprague-Dawley (SD) rats, and carefully isolated the small intestinal to collect the fresh rat mucus. And a SNE formulation (25 mg/ml in HBSS, 2 μL) was placed on the fresh mucus (200 μL), followed by a 30 min incubation at 37 °C. Movies were taken at a temporal resolution of 32.6 ms for 10 s using the LAS 4.5 software (Leica, Germany). The tracking resolution was about 10 nm, determined by gluing microspheres on microslides and tracking their apparent displacement by referring to a previous report [22,23]. The trajectories for $n = 100$ particles were analyzed using Image J, and three independent experiments were performed. Time averaged mean square displacement (MSD) and effective diffusivities (D*eff*) were calculated using the following equations:

$$\mathrm{MSD}_t = (x_t - x_0)^2 + (y_t - y_0)^2$$
$$Deff = \mathrm{MSD}/(4t)$$

(Where x and y represent the coordinates of the particle, and τ represent time scale or time lag).

2.7. Cellular uptake study

HT29-MTX-E12 (E12) cell were seeded on 12 plates at a density of 10×10^6/well, and maintained in Dulbecco's Modified Eagle's Medium (DMEM), supplemented with 10% fetal bovine serum. 1% non-essential amino acid, 1% penicillin - streptomycin. After cultivated for 3 days under 5% CO_2 at 37 °C, the E12 cell monolayers were slightly washed with Hank's balanced salt solution (HBSS), then treated with 500 μL SNEs (25 mg/mL in HBSS) for 1.5 h. Following incubation, cell monolayers were washed with HBSS and fixed with 4% paraformaldehyde, then stained with DAPI (5 μg/mL). Finally, the slides were embedded and observed under confocal laser scanning microscopy (CLSM) (Olympus FV1000, Japan).

The E12 cell monolayers were treated with 500 μL SNEs (25 mg/mL in HBSS) for 1.5 h. The upper medium were replaced by HBSS and washed for three times, followed by a 10 min lysis. Then lysis solution were collected to centrifuge at 4000 g for 10 min. Supernatant were collected, the particle numbers were calculated by Synergy H1m microplate reader, the total protein were measured by BCA assay kits.

2.8. Mucus penetration in E12 cells

The E12 cells were seeded at a density of 10×10^5 cells/mL on a polycarbonate membrane (pore size: 3 μm) in Costar Transwell 12-well plates (Corning Costar Corp.). Then E12 cell were cultured for 14–17 days. TEER value was measured before experiments. E12 monolayers were slightly washed for three times with HBSS and incubated for 1.5 h with 500 μL SNEs (25 mg/mL in HBSS) [24,25]. Following incubation, we slightly removed the formulations and washed E12 monolayers with HBSS. The polycarbonate membrane were cut and attached on the glass slides. Then stained with Hoechst and Alexa Fluor 488-conjugated WGA, respectively, and observed by CLSM using 63 × oil objective lens [26,27].

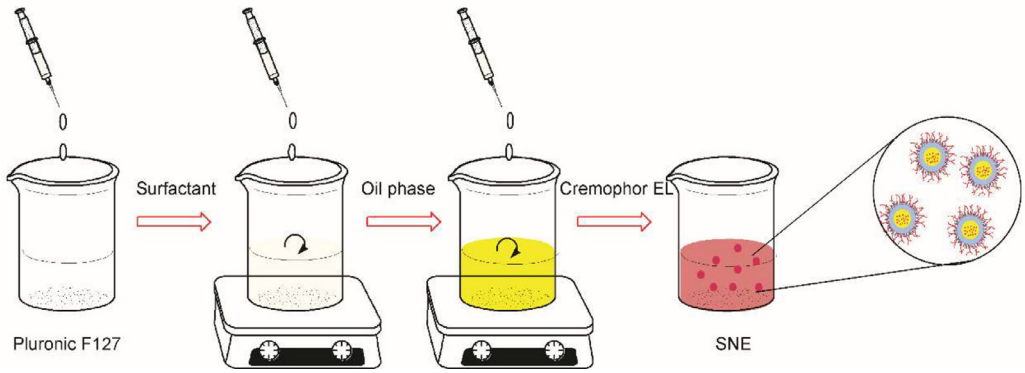

Fig. 1 – The reaction scheme of the preparation.

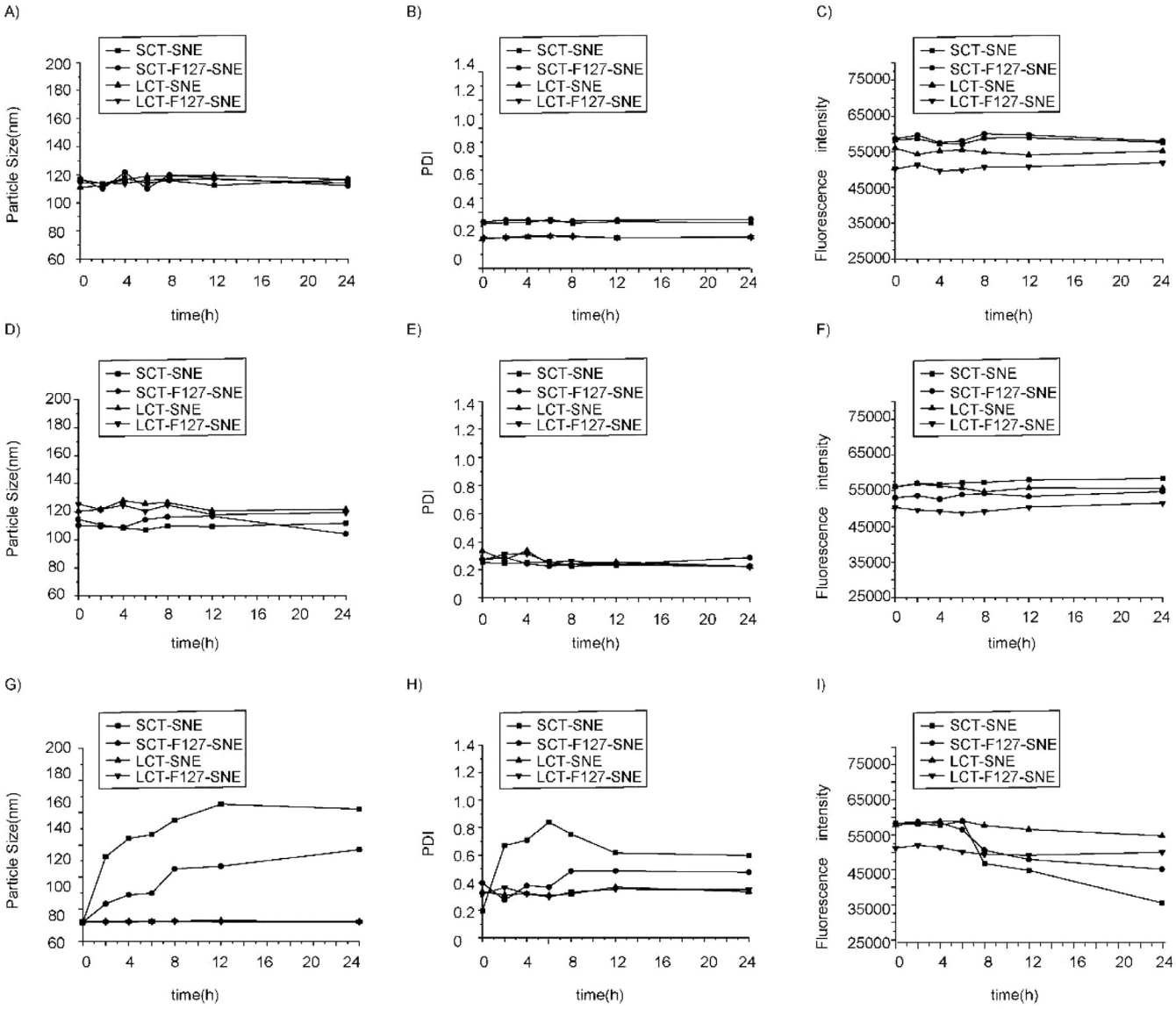

Fig. 2 – Changes of particle size, PDI and fluorescent intensity of SNEs in phosphate buffer saline (PBS) (A, B, C), simulated gastric fluid (SGF) (D, E, F) and simulated intestinal fluid (SIF) (G, H, I).

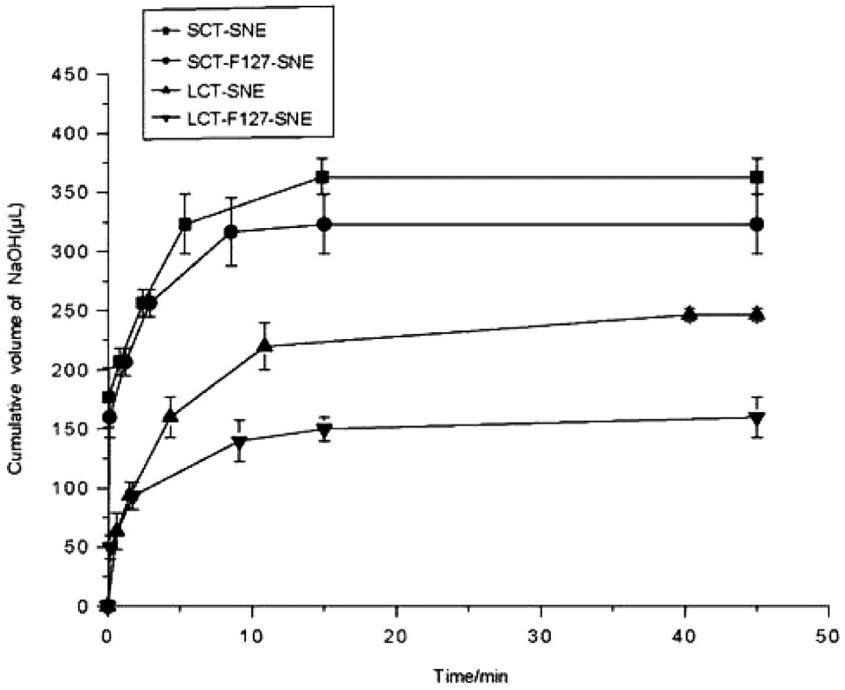

Fig. 3 – *In vitro* digestion curve for formulations comprising LCT and SCT. (■) SCT-SNE, (•) SCT-F127-SNE, (▲) LCT-SNE, (▼) LCT-F127-SNE. Each system contained 100 mg SNEs formulation ($n = 3$).

Table 1 – Particle size, polydispersity index (PDI) and z-potential of SNEs.

Formulation	Hydrodynamic diameter (nm)	PDI	Zeta potential (mV)
SCT-SNE	108.3 ± 2.4	0.248	−20.8 ± 3.4
SCT-F127-SNE	106.3 ± 2.9	0.202	1.0 ± 3.1
LCT-SNE	107.9 ± 7.0	0.179	−19.4 ± 3.4
LCT-F127-SNE	106.6 ± 2.6	0.196	−7.4 ± 1.9

Data are mean ± SD.

2.9. *Nanoparticle distribution in rat small intestine*

The absorption of intestinal villi was observed in male SD rats. All animal experiments were carried out according to the Institutional Animal Care and Use Committee (IACUC) guidelines of the Shanghai Institute of Materia Medica (IACUC code: 2016-05-GY-23). Male SD rats were fasted for 12 h before experiments, but allowed free access to water. We anesthetized male SD rats with urethane solution, and the ileum was exposed from a small incision in the abdomen. A 2 cm region was ligated by medical suture, and 400 μL SNEs (25 mg/mL in HBSS) was slowly injected into the loop [28]. After incubated for 1.5 h, the intestine was fixed with 4% paraformaldehyde solution for 3 h and dehydrated in 30% sucrose solution overnight at 4 °C. The tissue was frozen in Opti-mum cutting Temperature Compound (OTC). Finally, the intestines were sliced at a depth of 20 μm using a frizzing microtome (Leica CM1950, Germany), stained with DAPI and embedded for observed by CLSM.

2.10. *Pharmacokinetic study*

Twenty-four male SD rats weighing 275 ± 25 g were used for the pharmacokinetic study. SD rats were fasted for 12 h with free access to water and were randomly divided into four groups ($n = 6$ for each group). Rats were orally administered with SCT-SNE, SCT-F127-SNE, LCT-SNE and LCT-F127-SNE at a dose of 10 mg/kg. Blood samples (0.4 mL) were collected from the retro-orbital plexus at time points of 0.5, 1, 2, 4, 6, 8, 12 and 24 h. Fresh rat blood samples were stored at −20 °C.

Concentration of CsA were measured by HPLC, using previous report with slight modifications [18,29,30]. Firstly, we added acetonitrile (20 μL) and CsD (20 μL, 50 μg/ mL, internal standard) into samples, mixed for 5 min, then added 25 mg sodium fluoride. After shaking for 5 min, the samples were incubated in water bath at 45 °C for 15 min and shaken again. Finally, 4 mL tert–butyl methyl ether were added and mixed for 15 min to extract CsA and CsD. After centrifugation (4000 rpm, 10 min), the upper organic solution was collected and dried under nitrogen at 40 °C. The samples were dissolved into 100 μL solvent mixture (acetonitrile and phosphoric acid (pH 1.9) (6/4, v/v)) and 800 μL n-hexane, then centrifuged at 4000 rpm for 10 min. The upper organic phase were removed, 20 μL samples were injected into the HPLC for analysis. Data was analyzed by DAS 2.0 (USA) using non-compartment model.

An Agilent 1200 series HPLC system (Agilent, USA) and Zorbax SB-C18 (5 μm, 4.6 × 150 mm, Agilent, USA) were used to quantify CsA and CsD. The mobile phase consisted of acetonitrile, phosphoric acid (pH 1.9) and tert–butyl methyl ether (47/48/5, v/v/v). The flow rate was 1.5 mL/min. The

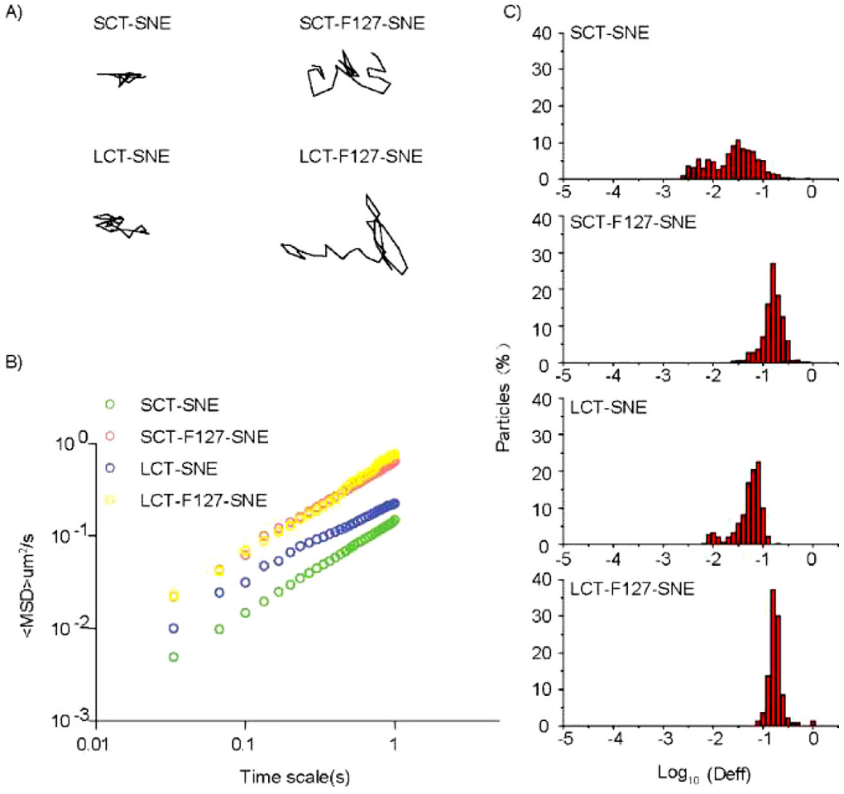

Fig. 4 – The transport of SNEs with different composition in fresh rat intestinal mucus at 37 °C. (A) Representative trajectories of particle motion in 1 s. (B) (MSD) values as a function of time. (C) Distributions of the logarithms of individual particle effective diffusivities (D_{eff}) on a time scale of 1 s. The data represent three independent experiments, which each tracked 100 NPs.

Table 2 – HPLC analysis of Cyclosporine A (CsA) in lipid digestion experiments *in vitro*.

Parameter	SCT-SNE	SCT-F127-SNE	LCT-SNE	LCT-F127-SNE
% in AP	39.5	47.8	68.4	87.3
% in precipitate	60.5	52.2	31.6	12.7
% in oil	No oil phase	No oil phase	No oil phase	No oil phase
% digestion	~99.5	~96.8	~95.0	~93.9

The concentration of Cyclosporine A (CsA) after 30 min digestion of 100 mg SCT, or LCT from SNEs by using digestion model. AP: aqueous phase.

column temperature was set at 70 °C. Samples were analyzed at 210 nm by UV.

3. Results and discussion

3.1. *Preparation and characterization of SNEs*

The compositions of SNEs are listed in supplementary Table S1. Short (SCT) and long (LCT) chain triglycerides, as oil phase, were widely used to prepare different SNE formulations. Ethanol and 1,2-propanediol increase the solubility of CSA. Cremophor EL has good capacity for self-emulsify. The SNEs are further synthesized according to Fig. 1. The particles size, polydispersity index and zeta potential of different SNEs are shown in Table 1. The samples had an average particle size

Table 3 – Pharmacokinetic parameters of CsA following oral administration of SNEs.

Formulation	C_{max}(μg/L)	T_{max}(h)	$AUC_{0\text{-}24}$(μg.h/L)
SCT-SNE	1315.3 ± 145.1	1.5	14,910.2 ± 1685.0***
SCT-F127-SNE	2176.7 ± 383.8	1.5	22,192.0 ± 1649.1***
LCT-SNE	1707.6 ± 119.3	1.0	18,212.2 ± 2436.5***
LCT-F127-SNE	3205.9 ± 533.8	0.9	32,215.9 ± 4613.8

AUC0–24h: The area under the blood drug concentration–time curve.
Cmax: The maximal blood concentration of drug.
Tmax: The time taken to reach the Cmax.
Statistically different when compared with the data of LCT-F127-SNE. (***$P < 0.001$, One-way ANOVA with Bonferroni's test).

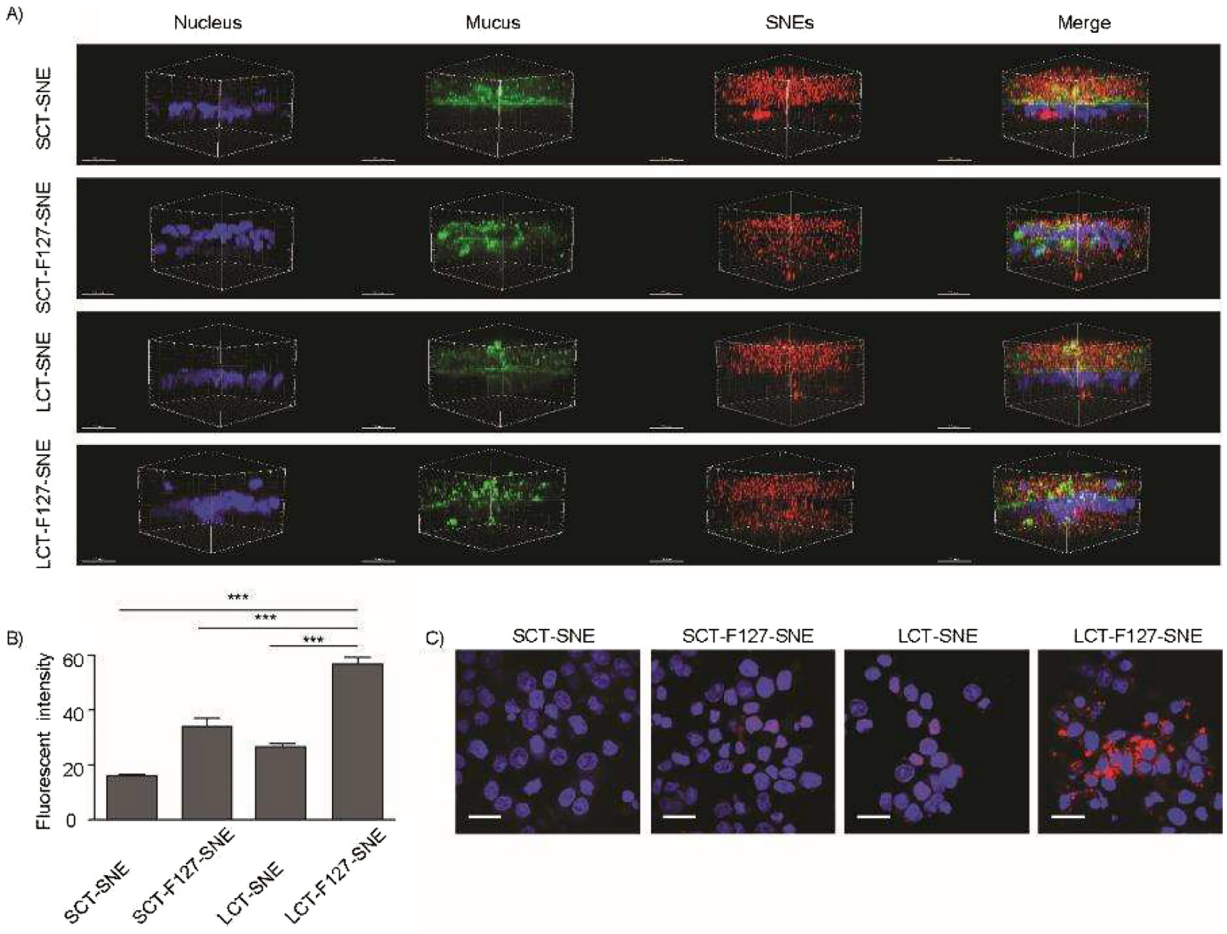

Fig. 5 – (A) 3D image of mucus penetration in E12 cell monolayers. (DAPI (blue), Alexa Fluor 488-WGA (green) and DiI (red) signals represent the cell nuclei, mucus and SNEs, respectively). Scale bar: 20 μm. (B) Cellular uptake of SNEs ($n = 3$) in E12 cell monolayers; (*$p < .001$ for the indicated comparison, One-way ANOVA with Bonferroni's test). (C) Representative images for SNEs cellular uptake by LSCM in E12 cell monolayers. LCT-F127-SNE exhibited the most effective cellular uptake (DAPI (blue) and DiI (red) signals represent the cell nuclei and SNEs, respectively). Scale bar: 20 μm. (For interpretation of the references to color in this figure legend, the reader is referred to the web version of this article.)**

of approximately 106.0 nm, and no significant change in particle size was found with F127 modification. The zeta potentials of SCT-SNE and LCT-SNE were approximately −20.0 mV; however, F127 modification increased zeta potential to 1.0 mV and −7.4 mV, respectively. The increased of zeta potential indicated that the extension of the hydrophilic polyethylene oxide (PEO) chains coated the oil phase surface, which had increased the hydrophilicity of SNEs and shielding of surface charges.

3.2. *Stability of fluorescently labeled SNEs*

It is highly crucial to ensure the stability of SNEs particles before conducting *in vitro* and *in vivo* studies. Therefore, we selected buffer and bio-relevant media such as PBS, SGF and SIF to test the stability of SNEs. An authentic assessment should lie on the stability of fluorescence since the undesired leakage of dyes from SNEs can reflect whether the nanoemulsion has been broken down or not. As shown in Fig. 2, little changes in fluorescence intensity, particle size, and PDI were observed in PBS and SGF buffers after 24 h, indicating the SNEs did not experience obvious structure damage. However, SCT-SNE and SCT-F127-SNE had approximately 35.7−48.2% reduction in fluorescence in SIF buffer, and the particle size and PDI increased dramatically. We attributed that these phenomena might be due to presence of short chain oil, which would be digested easily by lipase in intestinal environment. These results proved that lipolysis rate was dependent on the length of the fatty acid chains, the regime of which was the longer the fatty acid chains, the slower the digestion rate. Meanwhile, the F127 modified formulations were found to be more stable.

3.3. *In vitro digestion*

The *in vitro* digestion results suggested that the type of lipid and surface modification could influence the digestion rate. Our results showed that the LCT-SNEs were not completely lipolyzed after 35 min of digestion, while the SCT-SNEs had completely been lipolyzed, indicating that the long chain

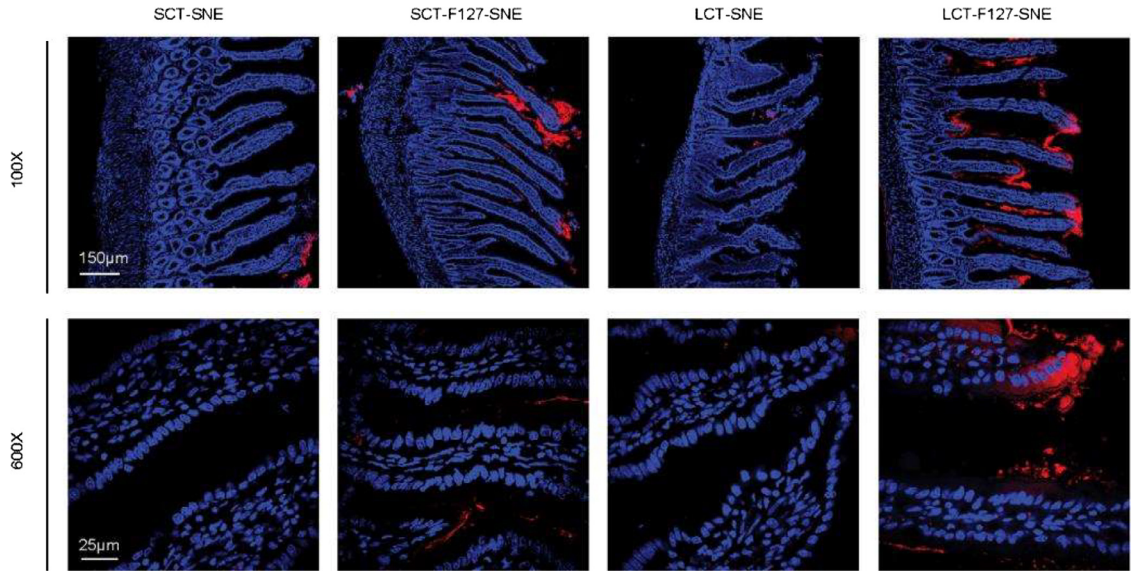

Fig. 6 – The distribution of DiI-labeled SNEs in rat intestinal after incubation 2 h, LCT-F127-SNE exhibited effective intestinal absorption in the studied intestinal sections, with more red fluorescence observed under LSCM. DAPI (blue) and DiI (red) signals represent the cell nuclei and SNEs, respectively. Scale bar: 150 μm and 25 μm. (For interpretation of the references to color in this figure legend, the reader is referred to the web version of this article.)

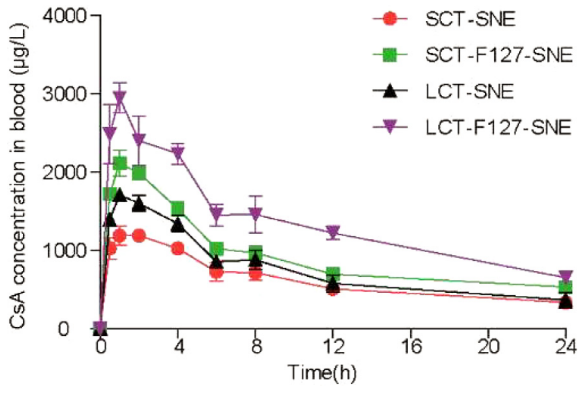

Fig. 7 – Mean plasma concentration versus time profiles of CsA after single oral administration of SNEs at a dose of 10 mg/kg, data were expressed as mean ± SD ($n = 6$).

oil had superior resistance against enzymatic degradation. When decorated with 5% F127, the digestion rate of SNEs was attenuated. The cumulative volume of NaOH (1 M) required for titration at different time-point is shown in Fig. 3. For the *In vitro* digestion test, titration curve was used to assess the lipid digestion rates. The results indicated that SNEs were digested more rapidly than SNEs decorated with 5% F127. We can conclude that the LCT-F127-SNE can resist digestion. The impact of SNEs on drug distribution after digestion *in vitro* was shown in Table 2. Approximately 60.5%, 52.2%, 31.6% and 12.7% of CsA precipitated from SCT-SNE, SCT-F127-SNE, LCT-SNE and LCT-F127-SNE, respectively. Less drug precipitation from LCT-F127-SNE suggested that LCT-F127-SNE was highly effective in preventing lipid digestion.

3.4. *Multi-Particle tracking in rat intestinal mucus in vitro*

We used multi-particle tracking (MPT) to measure the transport dynamics of fluorescence-labeled SNEs in fresh rat intestinal mucus. The results indicated that SCT-SNE and LCT-SNE without F127 modification had a weak diffusive capacity, and were completely trapped in the mucus. Whereas SNEs modified with 5% F127 exhibited increased diffusivity in the mucus. The movement of SCT-SNE and LCT-SNE were strongly hindered in fresh rat intestinal mucus, while SCT-F127-SNE and LCT-F127-SNE rapidly diffused in mucus layer (Fig. 4A). The time scale-dependent ensemble means squared displacement (MSD) values of the SNEs were quantified to evaluate the extent of impediment to particle transport (Fig. 4B). On a time scale of 1 s, MSD value of SCT-F127-SNE and LCT-F127-SNE were approximately 4-fold higher than those of SCT-SNE and LCT-SNE, respectively. We then characterized the distribution of individual particle effective diffusivities (*Deff*) on a time scale of 1 s (Fig. 4C). The results showed that most particles of SCT-F127-SNE and LCT-F127-SNE exhibited *Deff* values exceeding 0.1 $\mu m^2/s$. In contrast, only few particles of SCT-SNE and LCT-SNE diffused at a speed 0.1 $\mu m^2/s$ or faster.

3.5. *Cellular uptake studies*

Mucus-secreting E12 cell monolayer was adopted as the *in vitro* model of multiple barriers to take consideration of both mucus layer and epithelia. In order to quantify as well as visualize the uptake efficiency of the SNEs, we labeled them with DiI in the oil phase during the fabrication. After incubating the SNE with E12 cells for 1.5 h, LCT-F127-SNE exhibited the highest amount regarding both mucus penetration and cellular

uptake (Fig. 5A & 5C), with an uptake amount number (via BCA analysis) of 3.5-fold, 2.1-fold and 1.7-fold higher than that of SCT-SNE, LCT-SNE and SCT-F127-SNE, respectively (Fig. 5B). In accordance with the tracking results, we found that the modification of F127 was a critical determinant as well, while the length of fatty acid chain again appeared to be the secondary factor (Fig. 4 & 5). These evidences clearly addressed the crucial role of mucus layer in the multiple barriers that F127 plus longer fatty acid chain could significantly facilitate the SNEs to traverse the mucus, resulting to a considerable cellular uptake amount. Together with the digestion studies, these results provided promising indications that LCT-F127-SNE could be effectively absorbed by the intestine and could enhance the bioavailability of pharmaceuticals.

3.6. *Absorption across intestinal villi*

To confirm whether the above-mentioned data were good estimations of the *in vivo* behaviors of SNEs, we observed the intestinal uptake by CLSM. As shown in Fig. 6, stronger red fluorescence signal was observed in loops incubated with DiI-labeled LCT-F127-SNE, implying strong attachment to villi. The results indicated their resistance to lipase and rapid transport across the mucus layer due to the F127 modification that led to their effective absorption *in vivo*. Therefore, LCT-F127-SNE was further proved to be able to delivery oral drugs with high efficiency.

3.7. *Pharmacokinetic study*

To evaluate the absorption of CsA-loaded SENs *in vivo*, pharmacokinetics study was conducted in SD rat. The mean plasma concentration time curve is shown in Fig. 7. The pharmacokinetic parameters were summarized in Table 3. The efficient oral absorption of CsA was achieved by modifying SNEs with F127, the $AUC_{0\text{-}24}$ for LCT-F127-SNE was approximately 2.43-fold, 1.80-fold and 1.33-fold higher than SCT-SNE, LCT-SNE and SCT-F127-SNE, respectively. Similarly, the LCT-F127-SNE had the best $C_{max.}$ Overall, the results showed that the F127-SNEs conceal their recognition from enzyme, and smartly breached the mucus barrier. As a result, F127-SNEs could able to improve the oral bioavailability of PWSD.

4. Conclusion

In this study, we reasonably designed and investigated multifunctional SNE formulations for oral delivery of poorly water-soluble drugs. The SCT-F127-SNE and LCT-F127-SNE had nearly neutral surface charge and better stability in different bio-relevant media. The presence of a hydrophilic group (F127) on the surface of the lipid droplet generated a steric hindrance and reduced enzymatic degradation in the gastrointestinal tract. Moreover, F127 greatly improved the mucus-penetrating ability of SNEs. The above-mentioned attributes made LCT-F127-SNE efficient for their improved cellular uptake. Furthermore, efficient oral absorption of CsA was achieved by the LCT-F127-SNE, with 2.43-fold, 1.33-fold, 1.80-fold higher $AUC_{0\text{–}24\ h}$ values compared to those of CsA preparations, respectively. We demonstrated that our SNEs were able to effectively overcome the oral absorption barriers and will be a promising platform for oral delivery.

Conflicts of interest

The authors have no conflicts of interest to declare.

Acknowledgments

We are grateful for financial support received from the National Natural Science Foundation of China (81373356, 81573378 and 81703436), the Science and Technology Innovation Action Plan for Basic Research of Shanghai 2014 (14JC1493200) and CASIMM0120153020, Shanghai Sailing Program 2017(17YF1423500).

Supplementary materials

Supplementary material associated with this article can be found, in the online version, at doi:10.1016/j.ajps.2018.03.001.

REFERENCES

[1] Ha E-S, Kim J-S, Baek I-h, Hwang S-J, Kim M-S. Enhancement of dissolution and bioavailability of ezetimibe by amorphous solid dispersion nanoparticles fabricated using supercritical antisolvent process. J Pharm Investig 2015;45(7):641–9.
[2] Abuzara SM, Hyun SM, Kim JH, et al. Enhancing the solubility and bioavailability of poorly water-soluble drugs using supercritical antisolvent (SAS) process. Int J Pharm 2017.
[3] Parmar K, Patel J, Sheth N. Self nano-emulsifying drug delivery system for Embelin: design, characterization and in-vitro studies. Asian J Pharm Sci 2015;10(5):396–404.
[4] Porter CJ, Trevaskis NL, Charman WN. Lipids and lipid-based formulations: optimizing the oral delivery of lipophilic drugs. Nat Rev Drug Discov 2007;6(3):231–48.
[5] Shakeel F, Iqbal M, Ezzeldin E. Bioavailability enhancement and pharmacokinetic profile of an anticancer drug ibrutinib by self-nanoemulsifying drug delivery system. J Pharm Pharmacol 2016;68(6):772–80.
[6] Feeney OM, Crum MF, McEvoy CL, et al. 50years of oral lipid-based formulations: provenance, progress and future perspectives. Adv Drug Deliv Rev 2016;101:167–94.
[7] Feeney OM, Williams HD, Pouton CW, Porter CJ. 'Stealth' lipid-based formulations: poly(ethylene glycol)-mediated digestion inhibition improves oral bioavailability of a model poorly water soluble drug. J Control Rel 2014;192:219–27.
[8] Williams HD, Sassene P, Kleberg K, et al. Toward the establishment of standardized *in vitro* tests for lipid-based formulations, part 1: method parameterization and comparison of *in vitro* digestion profiles across a range of representative formulations. J Pharm Sci-US 2012;101(9):3360–80.
[9] Devraj R, Williams HD, Warren DB, Mohsin K, Porter CJ, Pouton CW. *In vitro* assessment of drug-free and fenofibrate-containing lipid formulations using dispersion and digestion testing gives detailed insights into the likely fate of formulations in the intestine. Eur J Pharm Sci 2013;49(4):748–60.

[10] Zhao L, Wei Y, Huang Y, He B, Zhou Y, Fu J. Nanoemulsion improves the oral bioavailability of baicalin in rats: *in vitro* and *in vivo* evaluation. Int J Nanomed 2013;8:3769–79.
[11] Delorme V, Dhouib R, Canaan S, Fotiadu F, Carriere F, Cavalier JF. Effects of surfactants on lipase structure, activity, and inhibition. Pharm Res 2011;28(8):1831–42.
[12] Sek L, Porter CJH, Charman WN. Characterisation and quantification of medium chain and long chain triglycerides and their *in vitro* digestion products, by HPTLC coupled with in situ densitometric analysis. J Pharm Biomed 2001;25(3-4):651–61.
[13] Porter CJ, Kaukonen AM, Boyd BJ, Edwards GA, Charman WN. Susceptibility to lipase-mediated digestion reduces the oral bioavailability of danazol after administration as a medium-chain lipid-based microemulsion formulation. Pharm Res 2004;21(8):1405–12.
[14] Lai SK, Wang YY, Hanes J. Mucus-penetrating nanoparticles for drug and gene delivery to mucosal tissues. Adv Drug Deliver Rev 2009;61(2):158–71.
[15] Johansson ME, Larsson JM, Hansson GC. The two mucus layers of colon are organized by the MUC2 mucin, whereas the outer layer is a legislator of host-microbial interactions. Proc Natl Acad Sci U S A 2011;108(Suppl 1):4659–65.
[16] Johansson MEV, Phillipson M, Petersson J, Velcich A, Holm L, Hansson GC. The inner of the two Muc2 mucin-dependent mucus layers in colon is devoid of bacteria. Proc Natl Acad Sci U S A 2008;105(39):15064–9.
[17] Liu M, Zhang J, Shan W, Huang Y. Developments of mucus penetrating nanoparticles. Asian J Pharm Sci 2015;10(4):275–82.
[18] Chen D, Xia D, Li X, et al. Comparative study of Pluronic((R)) F127-modified liposomes and chitosan-modified liposomes for mucus penetration and oral absorption of cyclosporine A in rats. Int J Pharm 2013;449(1-2):1–9.
[19] Xia F, Fan W, Jiang S, et al. Size-dependent translocation of nanoemulsions via oral delivery. ACS Appl Mater Interfaces 2017;9(26):21660–72.
[20] Hu X, Zhang J, Yu Z, et al. Environment-responsive aza-BODIPY dyes quenching in water as potential probes to visualize the *in vivo* fate of lipid-based nanocarriers. Nanomedicine 2015;11(8):1939–48.
[21] Han SF, Yao TT, Zhang XX, et al. Lipid-based formulations to enhance oral bioavailability of the poorly water-soluble drug anethol trithione: effects of lipid composition and formulation. Int J Pharm 2009;379(1):18–24.
[22] Apgar J, Tseng Y, Fedorov E, Herwig MB, Almo SC, Wirtz D. Multiple-particle tracking measurements of heterogeneities in solutions of actin filaments and actin bundles. Biophys J 2000;79(2):1095–106.
[23] Suh J, Dawson M, Hanes J. Real-time multiple-particle tracking: applications to drug and gene delivery. Adv Drug Deliv Rev 2005;57(1):63–78.
[24] Zhu X, Wu J, Shan W, Zhou Z, Liu M, Huang Y. Sub-50 nm nanoparticles with biomimetic surfaces to sequentially overcome the mucosal diffusion barrier and the epithelial absorption barrier. Adv Funct Mater 2016;26(16):2728–38.
[25] Shan W, Zhu X, Liu M, et al. Overcoming the diffusion barrier of mucus and absorption barrier of epithelium by self-assembled nanoparticles for oral delivery of insulin. ACS Nano 2015;9(3):2345–56.
[26] Li X, Guo S, Zhu C, et al. Intestinal mucosa permeability following oral insulin delivery using core shell corona nanolipoparticles. Biomaterials 2013;34(37):9678–87.
[27] Mura S, Hillaireau H, Nicolas J, et al. Biodegradable nanoparticles meet the bronchial airway barrier: how surface properties affect their interaction with mucus and epithelial cells. Biomacromolecules 2011;12(11):4136–43.
[28] Yu M, Wang J, Yang Y, et al. Rotation-facilitated rapid transport of nanorods in mucosal tissues. Nano Lett 2016;16(11):7176–82.
[29] Xia D, Yu H, Tao J, et al. Supersaturated polymeric micelles for oral cyclosporine a delivery: the role of Soluplus-sodium dodecyl sulfate complex. Colloids surf B, Biointerfaces 2016;141:301–10.
[30] Guada M, Lasa-Saracibar B, Lana H, Dios-Vieitez Mdel C, Blanco-Prieto MJ. Lipid nanoparticles enhance the absorption of cyclosporine A through the gastrointestinal barrier: *In vitro* and *in vivo* studies. Int J Pharm 2016;500(1-2):154–61.